ARTICLE

Fluoroalkylated Silicon-Containing Surfaces—Estimation of Solid-Surface Energy

Shreerang S. Chhatre,[†] Jesus O. Guardado,[‡] Brian M. Moore,[§] Timothy S. Haddad,[||] Joseph M. Mabry,[§] Gareth H. McKinley,*[,⊥] and Robert E. Cohen*[,†]

Department of Chemical Engineering, Department of Mechanical Engineering, and Department of Materials Science and Engineering, Massachusetts Institute of Technology, Cambridge, Massachusetts 02139, United States, Space and Missile Propulsion Division and ERC Incorporated, Air Force Research Laboratory, Edwards Air Force Base, California 93524, United States

ABSTRACT The design of robust omniphobic surfaces, which are not wetted by low-surface-tension liquids such as octane (γ_{lv} = 21.6 mN/m) and methanol (γ_{lv} = 22.7 mN/m), requires an appropriately chosen surface micro/nanotexture in addition to a low solid-surface energy (γ_{sv}). 1H,1H,2H,2H-Heptadecafluorodecyl polyhedral oligomeric silsesquioxane (fluorodecyl POSS) offers one of the lowest solid-surface energy values ever reported ($\gamma_{sv} \approx 10$ mN/m) and has become the molecule of choice for coating textured surfaces. In this work, we synthesize and evaluate a series of related molecules that either retain the POSS cage and differ in fluoroalkyl chain length or that retain the fluorodecyl chains surrounding a linear or cyclic molecular structure. The solid-surface energy (γ_{sv}) of these molecules was estimated using contact angle measurements on flat spin-coated silicon wafer surfaces. Zisman analysis was performed using a homologous series of n-alkanes ($15.5 \leq \gamma_{lv} \leq 27.5$ mN/m), whereas Girifalco—Good analysis was performed using a set of polar and nonpolar liquids with a wider range of liquid surface tension ($15.5 \leq \gamma_{lv} \leq 72.1$ mN/m). The hydrogen-bond-donating, hydrogen-bond-accepting, polar, and nonpolar (dispersion) contributions to the solid-surface energy of each compound were determined by probing the surfaces using a set of three liquid droplets of either acetone, chloroform, and dodecane or diiodomethane, dimethyl sulfoxide, and water.

KEYWORDS: superhydrophobicity • oleophobicity • solid-surface energy • Zisman analysis • Girifalco—Good method

INTRODUCTION

In the recent past, there have been a number of reports on surfaces that are not wetted by liquid droplets, i.e., superhydrophobic (1—4), oleophobic (5—15), hygrophobic (16), and omniphobic (7, 12) surfaces. These surfaces have potential applications in oil—water separation, nonwettable textiles (2, 3, 6, 8, 9, 14, 15), and fingerprint/smudge resistant touch-screen devices. Here we use the term omniphobicity to refer to surfaces that are not wetted by a broad set of liquids, including water, alkanes, alcohols, acids, bases, and other organic liquids. The design of omniphobic surfaces involves selection of a suitable surface chemistry to minimize the solid-surface energy and optimal choice of the surface texture.

In our previous work, we emphasized re-entrant topography as a necessary condition for the design of surfaces that are not wetted by low-surface-tension liquids (7—9, 11—13). Liquids such as octane (γ_{lv} = 21.6 mN/m) and methanol (γ_{lv} = 22.7 mN/m) will partially wet a flat untextured surface (equilibrium contact angle, $\theta_E < 90°$) of any surface chemistry. Using a combination of surface chemistry and re-entrant texture, surfaces that exhibit substantially enhanced nonwettability to such liquids (apparent contact angle, $\theta^* > 90°$) can be created. On such nonwetting surfaces, liquid droplets sit partially on the solid texture and partially on the air trapped between the asperities of the solid texture. The Cassie—Baxter (CB) relation can be used to understand variations in the apparent contact angles (θ^*) for liquid droplets with solid—liquid—air composite interfaces. The CB relation shows that the apparent contact angle (θ^*) increases as the equilibrium contact angle (θ_E) increases and as the relative amount of trapped air increases (17). We have also developed an expression for the breakthrough pressure (P_b) required for the disruption of this solid—liquid—air composite interface (or "CB state") (12). Both the apparent contact angle (θ^*) and the breakthrough pressure (P_b) increase monotonically with increasing equilibrium contact angle (θ_E) (7—9, 12). Therefore, maximizing θ_E is one objective in the optimal design of omniphobic surfaces with robust composite interfaces.

We have used fluorodecyl POSS-based coatings to design a range of robust nonwettable surfaces (7—9, 11—13). A fluorodecyl POSS molecule consists of a silicon—oxygen cage surrounded by eight 1H,1H,2H,2H-heptadecafluorodecyl chains (18). A flat silicon wafer spin-coated with a uniform coating of this molecule has one of the highest reported values of equilibrium contact angle for water

* Corresponding author. Tel.: (617) 253-3777 (R.E.C.); (617) 258-0754 (G.H.M.). Fax: (617) 258-8224 (R.E.C.); (617) 258-8559 (G.H.M.). E-mail: recohen@mit.edu (R.E.C.); gareth@mit.edu (G.H.M.).

Received for review August 13, 2010 and accepted October 21, 2010

[†] Department of Chemical Engineering, Massachusetts Institute of Technology.
[‡] Department of Materials Science and Engineering, Massachusetts Institute of Technology.
[§] Space and Missile Propulsion Division, Air Force Research Laboratory.
[||] ERC Incorporated, Air Force Research Laboratory.
[⊥] Department of Mechanical Engineering, Massachusetts Institute of Technology.

DOI: 10.1021/am100729j

2010 American Chemical Society

Published on Web 11/10/2010

Advancing contact angles (θ_{adv})	Water (γ_{lv} = 72.1 mN/m)	Diiodomethane (γ_{lv} = 50.8 mN/m)	Rapeseed Oil (γ_{lv} = 35.5 mN/m)	Hexadecane (γ_{lv} = 27.5 mN/m)	Octane (γ_{lv} = 21.6 mN/m)
Fluorodecyl POSS 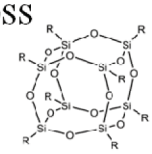	122 ± 2° 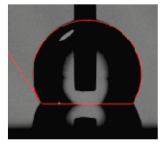	100 ± 2° 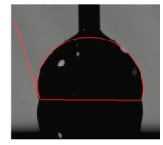	88 ± 3° 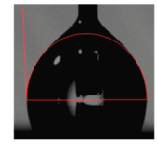	80 ± 1° 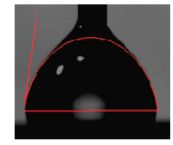	67 ± 1° 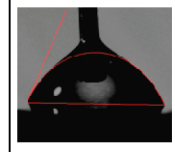
Tecnoflon 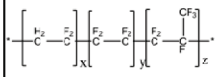	110 ± 2° 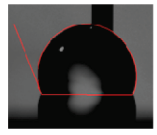	80 ± 2° 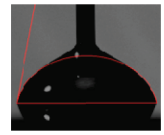	71 ± 2° 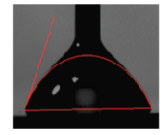	58 ± 2° 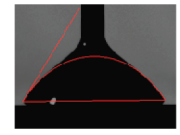	16 ± 3° 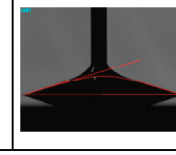

FIGURE 1. Variation of advancing contact angles (θ_{adv}) on flat silicon wafers spin-coated with fluorodecyl T_8 and Tecnoflon is shown. The advancing contact angles decrease in magnitude as the surface tension of the contacting liquids decreases from γ_{lv} = 72.1 mN/m (for water) to γ_{lv} = 21.6 mN/m (for octane) and as the solid-surface energy increases from fluorodecyl T_8 to Tecnoflon.

Table 1. Structure of Fluorohexyl T_8, Fluoropropyl T_8, Hexafluoro-i-butyl T_8 is shown along with the Structure of Fluorodecyl T_8 and Fluorooctyl T_8, Fluorodecyl Q_4, and Fluorodecyl M_2 for reference

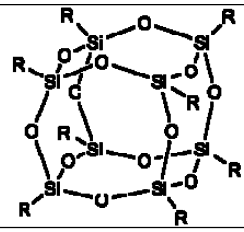	Fluorodecyl T_8, R = -$(CH_2)_2$-$(CF_2)_7$-CF_3
	Fluorooctyl T_8, R = -$(CH_2)_2$-$(CF_2)_5$-CF_3
	Fluorohexyl T_8, R = -$(CH_2)_2$-$(CF_2)_3$-CF_3
	Fluoropropyl T_8, R = -$(CH_2)_2$-CF_3
	Hexafluoro-*i*-butyl T_8, R = -CH_2-$CH(CF_3)_2$
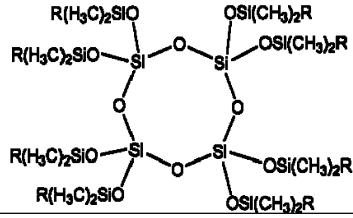	Fluorodecyl Q_4, R = -$(CH_2)_2$-$(CF_2)_7$-CF_3
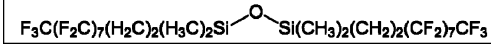	Fluorodecyl M2, R = -$(CH_2)_2$-$(CF_2)_7$-CF_3

droplets ($\theta_E \approx 122°$). Moreover, liquid droplets with a wide range of surface tension ($15.5 \leq \gamma_{lv} \leq 72.1$ mN/m) form high contact angles on a fluorodecyl POSS-coated flat surface (as summarized in Figure 1). The contact angles (θ_{adv} and θ_{rec}) are significantly higher on a fluorodecyl POSS surface than on a corresponding surface coated with a fluoropolymer such as Tecnoflon (BR 9151, a fluoro-elastomer from Solvay Solexis). In addition, it is apparent from Figure 1 that the difference between the corresponding contact angles on the two surfaces increases as the liquid surface tension (γ_{lv}) decreases. The molecular level origins of the unusually low wettability of fluorodecyl POSS remains unresolved.

In this study, we document the wettability of two sets of fluorinated silicon-containing molecules in an attempt to resolve some aspects of the unanswered questions regarding fluorodecyl POSS. In the first set, the length of the fluorinated chain is changed keeping the T_8 silicon/oxygen cage intact. [This cage is referred to generally as the T_8 cage because it has eight silicon atoms each bonded to three oxygen atoms.] In the other set of molecules, the fluorodecyl chain is retained and the silicon/oxygen architecture is changed successively from a T_8 cage to a Q_4 ring [four Si atoms, each bonded to four oxygen atoms] or a M_2 straight chain [two Si atoms, each bonded to a single oxygen atom]. The structure and chemical formulas of various molecules are summarized in Table 1.

The wettability of these materials is assessed using contact angle measurements on smooth spin-coated Si wafers with a set of probing liquids. There are various methods described in the literature to estimate the solid-surface energy from contact angle data: including the Zisman analysis (19), Owens−Wendt method (20), or Giri falco−Good method (21, 22). In this work, we perform Zisman analysis with a set of n-alkanes, a standard framework for quantifying nonwettability of low energy solid surfaces. We also estimate the surface energies of our solid

surfaces using the Girifalco−Good analysis, which additionally considers polar contributions in the wettability analysis. In the literature, the term "surface energy" is loosely used to indicate "surface energy per unit area" or "specific surface energy." In this article, we have continued to use the term "surface energy" with the understanding that it indeed means "specific surface energy," and it has units of mN/m or mJ/m^2.

EXPERIMENTAL DETAILS

Fluorodecyl POSS. A 94.3% yield of pure 1H,1H,2H,2H-heptadecafluorodecyl$_8$T$_8$ (fluorodecyl POSS) was obtained using a previously reported method (18).

Fluorooctyl POSS. A 95.1% yield of pure 1H,1H,2H,2H-tridecafluorooctyl$_8$T$_8$ (fluorooctyl POSS) was obtained using a previously reported method (18).

Fluorohexyl POSS. A 91.5% yield of pure 1H,1H,2H,2H-nonafluorohexyl$_8$T$_8$ (fluorohexyl POSS) was obtained using a previously reported method (18).

Fluoropropyl POSS. Fluoropropyl POSS was synthesized using a modification of a previously reported method (23). 3,3,3-Trifluoropropyltrichlorosilane (0.87 mL) was added to a stirred solution of heptakis(3,3,3-trifluoropropyl)tricycloheptasiloxane trisodium silanolate (4.00 g) in THF (70 mL) at room temperature. Triethylamine (0.49 mL) was then added dropwise to the mixture. The contents were stirred under nitrogen for 3 h in a 150 mL round-bottom flask with a Teflon-coated magnetic stir bar. After filtering the precipitated salts, the filtrate was concentrated under reduced pressure. The fine white powder formed was rinsed with methanol and dried. A 76% yield of pure 3,3,3-trifluoropropyl$_8$T$_8$ (fluoropropyl POSS) was obtained.

Hexafluoroisobutyl POSS. Hexafluoroisobutene (28.4 g, 173 mmol) was condensed into a 250 mL heavy- walled reaction vessel with a Teflon-coated magnetic stir bar. $HSiCl_3$ (23.9 g, 176 mmol) was then added at −10 °C under nitrogen followed by a 0.2 M H_2PtCl_6 isopropanol catalyst solution (0.5 mL, 0.1 mmol). The flask was sealed, heated to 150 °C, and stirred for 40 h. The contents were then vacuum transferred at 0 °C to a collection flask, which was then cooled to −80 °C. While slowly being warmed to −40 °C, volatiles were removed under static vacuum to give an 85% yield of hexafluoroisobutyltrichlorosilane (44.2 g, 148 mmol). ^{1}H NMR (δ, $CDCl_3$) 3.29 ppm (1H, nonet, $^3J_{H-F}$ and $^3J_{H-H}$ = 7.2 Hz, CH), 1.93 ppm (2H, d, $^3J_{H-H}$ = 7.2 Hz, CH_2); ^{19}F NMR (δ, $CDCl_3$) −68.23 ppm (d, $^3J_{H-F}$ = 7.2 Hz); ^{13}C{^{1}H} NMR (δ, $CDCl_3$) 123.28 ppm (quart, $^1J_{C-F}$ = 281 Hz, CF_3) 44.40 ppm (sept, $^2J_{C-F}$ = 30 Hz, CH), 18.49 (m, $^3J_{C-F}$ = 1.8 Hz, CH_2); ^{29}Si{^{1}H} NMR (δ, $CDCl_3$) 8.14 ppm (br, s).

Hexafluoroisobutyltrichlorosilane (44.19 g, 148 mmol) was placed into a 250 mL round-bottom flask (rbf) with a Teflon-coated magnetic stir bar under nitrogen and heated to 100 °C. Trimethylorthoformate (145.3 mL, 1.33 mol) was added dropwise over a period of 1.5 h and the reaction was refluxed overnight. 1H,1H,2H-Hexafluoroisobutyltrimethoxysilane was isolated by fractional distillation (bp =102 °C) under full dynamic vacuum, in 63% isolated yield (26.57 g, 93 mmol). ^{1}H NMR (δ, $CDCl_3$) 3.52 ppm (9 H, s, OMe), 3.06 ppm (1H, nonet, $^3J_{H-F}$ and $^3J_{H-H}$ = 7.2 Hz, CH), 0.97 ppm (2H, d, $^3J_{H-H}$ = 7.2 Hz, CH_2); ^{19}F NMR (δ, $CDCl_3$) −69.25 ppm (d, $^3J_{H-F}$ = 7.2 Hz); ^{13}C{^{1}H} NMR (δ, $CDCl_3$) 123.75 ppm (quart, $^1J_{C-F}$ = 269 Hz, CF_3), 50.27 (s, OCH_3) 43.64 ppm (sept, $^2J_{C-F}$ = 29 Hz, CH), 3.20 (m, $^3J_{C-F}$ = 1.7 Hz, CH_2); ^{29}Si{^{1}H} NMR (δ, CDCl3) −48.7 ppm (s).

1H,1H,2H-Hexafluoroisobutyltrimethoxysilane (2.00 g, 7.00 mmol) and 205 mg of KOH solution (774 mg KOH in 100 mL H_2O) were added to 7 mL of ethanol in a 25 mL rbf with a Teflon-coated magnetic stir bar and stirred overnight at room temperature, under nitrogen. The fine white powder formed was rinsed with ethanol and dried. An 85% yield of pure Hexafluoroisobutyl POSS was obtained. ^{1}H NMR (δ, C_6F_6) 3.65 ppm (1H, nonet, $^3J_{H-F}$ and $^3J_{H-H}$ = 7 Hz, CH), 1.54 ppm (2H, d, $^3J_{H-H}$ = 7 Hz, CH_2); ^{19}F NMR (δ, C_6F_6) −70.4 ppm (d, $^3J_{H-F}$ = 7 Hz); ^{13}C{^{1}H} NMR (δ, C_6F_6) 123.47 ppm (quart, $^1J_{C-F}$ = 282 Hz, CF_3), 43.83 ppm (sept, $^2J_{C-F}$ = 30 Hz, CH), 5.18 (s, CH_2); ^{29}Si{^{1}H} NMR (δ, C_6F_6) −69.4 ppm (s).

1H,1H,2H,2H-Heptadecafluorodecyl$_8$M$_8$Q$_4$ (Fluorodecyl$_8$M$_8$Q$_4$). 1H,1H,2H,2H-Heptadecafluorodecyldimethylchlorosilane (25 g, 46.2 mmol), octakis[chloro calcium oxy]cyclotetrasilicate (24) (3.4 g, 3.7 mmol), acetone (50 mL), and AK225 (14 mL) were added to a 100 mL rbf and refluxed under nitrogen for 3 days (25). The volatiles were then removed under vacuum. The product was dissolved in AK225 solvent (50 mL) and a water extraction was used to remove $CaCl_2$. Isopropanol (10 mL) and Amberlyst 15 (1 g) were added after reducing the solvent to 25 mL. Amberlyst is a sulfonic acid catalyst based in a cross-linked styrene divinylbenzene polymeric resin. Amberlyst is commercially available, reusable, and nonhazardous. It works under heterogeneous conditions and can easily be removed by filtration. After 3 h of stirring, the solution was filtered through silica gel (1.20 g, 60 Å pore size, 35−75 μm particle size). After redissolving the product in AK225 (11 mL), Amberlyst 15 (1.03 g) and silica gel were added (26), and the mixture was stirred overnight at room temperature. The solution was filtered through silica gel, the volatiles were removed by dynamic vacuum, and a distillation to isolate the fluorodecyl$_2$M$_2$ disiloxane was performed (see below). The fluorodecyl$_8$M$_8$Q$_4$ was dissolved in a minimal amount of AK225. A white precipitate formed upon sitting at room temperature. The AK225 was filtered off and the solid was washed with chloroform. A 9% yield (1.5 g) of fluorodecyl$_8$M$_8$Q$_4$ was obtained. ^{29}Si{^{1}H} NMR (AK225, ppm) 12.0 (s), −108.3 (s).

1,3-bis(1H,1H,2H,2H-Heptadecafluorodecyl)-1,3-tetramethyldisiloxane (Fluorodecyl$_2$M$_2$ disiloxane). A distillation at 118 °C, 0.2 mmHg was performed during the synthesis of fluorodecyl$_8$M$_8$Q$_4$ to isolate fluorodecyl$_2$M$_2$ disiloxane. A 10% yield (4.7 g) of fluorodecyl$_2$M$_2$ disiloxane was obtained. ^{1}H NMR ($CDCl_3$, ppm) 0.12 (s), 0.75 (m), 2.03 (m). ^{29}Si{^{1}H} NMR ($CDCl_3$, ppm) 8.4 (s).

Surface Characterization. The fluoroalkylated silicon-containing molecules were dissolved in Asahiklin solvent (AK 225, Asahi Glass Company) at a concentration of 10 mg/mL. Later, the solutions were spin-coated on a flat silicon wafer at 900 rpm for 30 s to achieve uniformly coated flat surfaces (AFM rms roughness ∼10 nm, see Table S7 and Figure S5 in the Supporting Information) for contact angle measurements. Advancing and receding contact angles were measured using a VCA2000 goniometer (AST Inc.) with ∼5 μL droplets of various liquids (purchased from Aldrich and used as received).

RESULTS AND DISCUSSION

Zisman and co-workers introduced the concept of the critical surface tension for a solid surface (γ_c) (19, 27−38), and it has become the most commonly used parameter to rank order solid-surface energy (γ_{sv}) and wettability of different substrates. To assess the impact of molecular structure on wettability, we performed contact angle measurements on the full set of fluoroalkylated silicon-containing molecules shown in Table 1. n-Alkanes [pentane (γ_{lv} = 15.5 mN/m) to hexadecane (γ_{lv} = 27.5 mN/m)] were used as contacting liquids, and the advancing contact angles (θ_{adv}) results are summarized in Figure 2. Strong linear correlations (R^2 = 0.95−0.99) were observed for plots of cos θ_{adv} versus liquid surface tension (γ_{lv}). The critical surface tension (γ_c) for the spin-coated surfaces was obtained by a linear ex-

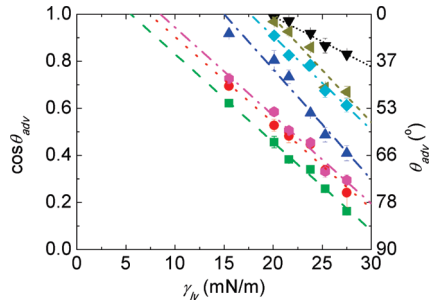

FIGURE 2. Zisman analysis for fluoroalkylated silicon-containing compounds. Cosine of advancing contact angles (θ_{adv}) for droplets of hexadecane (γ_{lv} = 27.5 mN/m), dodecane (γ_{lv} = 25.3 mN/m), decane (γ_{lv} = 23.8 mN/m), octane (γ_{lv} = 21.6 mN/m), heptane (γ_{lv} = 20.1 mN/m), and pentane (γ_{lv} = 15.5 mN/m) on a spin-coated film on a flat silicon wafer are plotted against the surface tension of contacting liquids (γ_{lv}). For fluorodecyl T_8 (γ_c = 5.5 mN/m, ■), fluorooctyl T_8 (γ_c = 7.4 mN/m, ●), fluorohexyl T_8 (γ_c = 8.5 mN/m, ⬢), fluoropropyl T_8 (γ_c = 19.7 mN/m, left-facing triangle), hexafluoroisobutyl T_8 (γ_c = 17.7 mN/m, ♦), fluorodecyl Q_4 (γ_c = 14.5 mN/m, ▲), and fluorodecyl M_2 (γ_c = 19.6 mN/m, ▼), the critical surface tension (γ_c) is obtained by a linear extrapolation of the corresponding best-fit line.

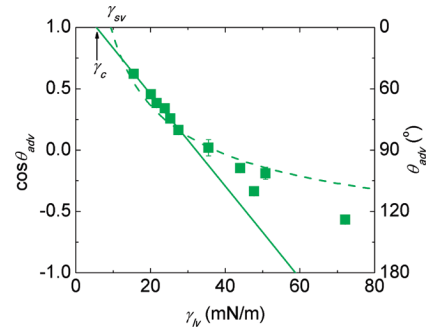

FIGURE 3. Variation in advancing contact angles (θ_{adv}) of liquid droplets with a wide range of surface tension on a fluorodecyl T_8 surfaces is shown in this figure. Cosine of advancing contact angles (θ_{adv}) for droplets of water (γ_{lv} = 72.1 mN/m), diiodomethane (γ_{lv} = 50.8 mN/m), ethylene glycol (γ_{lv} = 47.7 mN/m), dimethyl sulfoxide (γ_{lv} = 44 mN/m), rapeseed oil (γ_{lv} = 35.5 mN/m), hexadecane (γ_{lv} = 27.5 mN/m), dodecane (γ_{lv} = 25.3 mN/m), decane (γ_{lv} = 23.8 mN/m), octane (γ_{lv} = 21.6 mN/m), heptane (γ_{lv} = 20.1 mN/m), and pentane (γ_{lv} = 15.5 mN/m) on a spin-coated film on a flat silicon wafer are plotted against the surface tension of contacting liquids (γ_{lv}). The Zisman best fit line for the alkane data (—) and the best fit Girifalco-Good curve (- - -) over the whole range of liquids is shown with the respective intercepts γ_c = 5.5 mN/m, and γ_{sv} = 9.3 mN/m, respectively.

trapolation of the best-fit line through the cos θ_{adv} versus γ_{lv} data. The intercept of this extrapolation to the cos θ_{adv} = 1 line is the critical surface tension (γ_c). As the length of the perfluorinated chain decreased from fluorodecyl T_8 (■) to fluoropropyl T_8 (left-facing triangle), the critical surface tension (γ_c) increased monotonically from 5.5 to 19.7 mN/m. This trend is consistent with Zisman's results on modified poly tetrafluoroethylene (PTFE) (37), chlorinated polymers (31), fluorinated (meth)acrylate polymers (35), and perfluorinated carboxylic acids (29, 33, 34). Additionally, the critical surface tension (γ_c) increased as the size and complexity of the −Si/O− structure decreased; from γ_c = 5.5 mN/m for the fluorodecyl T_8 (cage, ■) to γ_c = 14.5 mN/m for the fluorodecyl Q_4 (ring, ▲) and γ_c = 19.6 mN/m for the fluorodecyl M_2 (straight chain,▼).

The critical surface tension (γ_c) is a qualitative indicator of the solid-surface energy (γ_{sv}) but it is not equal to the solid-surface energy ($\gamma_c \neq \gamma_{sv}$). Any liquid with a lower surface tension than the critical surface tension ($\gamma_{lv} < \gamma_c$) is expected to completely wet the solid surface ($\theta_E \approx 0$). Zisman noted that the critical surface tension (γ_c) can change if a different set of probing liquids is used on the same solid surface. When the solid surface and/or the contacting liquid is polar with a higher value of surface tension, the contact angle data deviate from the linear trend, as shown in Figure 3 for a flat silicon wafer spin-coated with fluorodecyl T_8. The advancing contact angle data (θ_{adv}, ■) for liquids with a wider range of surface tensions (15.5 ≤ γlv ≤ 72.1 mN/m) are plotted along with the linear extrapolation of the Zisman line (solid line). The Zisman line fits the alkane data well (R^2 = 0.99 for fluorodecyl T_8, Figure 2, γ_{lv} ≤30 mN/m); however, it deviates significantly when other liquids are included (R^2 = 0.04 for fluorodecyl T_8, Figure 3). Alkanes are completely nonpolar, whereas higher-surface-tension liquids like water, ethylene glycol, or dimethyl sulfoxide have polar functional groups, and the polarity of these probing liquids is considered to be the cause of deviation from the Zisman line.

A better model that incorporates the polarity of the solid surface and/or the contacting liquid was proposed by Girifalco, Good and co-workers (21, 22, 39−43). According to this framework, the solid-surface energy (γ_{sv}) is given by eq 1, where θ_E is the equilibrium contact angle and φ_{sl} is a solid−liquid interaction parameter

$$W_{sl}^a = \gamma_{lv}(1 + \cos\theta_E) = 2\phi_{sl}\sqrt{\gamma_{sv}\gamma_{lv}} \qquad (1)$$

Equation 1 has two unknowns, γ_{sv} and φ_{sl}. The parameter φ_{sl} equals the ratio of work of adhesion of the solid−liquid pair (W_{sl}^a) to the square roots of the works of cohesion of the solid ($W_{ss}^c = 2\gamma_{sv}$) and the liquid ($W_{ll}^c = 2\gamma_{lv}$), where $W_{ss}^c W_{ll}^c = 4\gamma_{sv}\gamma_{lv}$. The Berthelot geometric mean mixing rule suggests that the work of adhesion can be approximated as the product of the square roots of the two works of cohesion (22). For nonpolar liquid droplets on nonpolar solids, this is indeed the case ($W_{sl}^a = \sqrt{W_{ss}^c W_{ll}^c}$), and the solid−liquid interactions are nearly ideal ($\varphi_{sl} = W_{sl}^a/\sqrt{W_{ss}^c W_{ll}^c} = 1$), e.g., alkane droplets on fluorodecyl POSS (Figures 2 and 3). However, in general, the value of φ_{sl} for a solid−liquid pair is not known a priori. Contact-angle measurements were performed over a broad range of liquids with differing polarities, and the average value of φ_{sl} was assumed to be unity. The advancing contact angle measurement results, along with the (φ_{sl} = 1) best fit Girifalco−Good curve (- - ■) are shown in Figure 3 for a fluorodecyl T_8 surface. Alkanes from pentane (γ_{lv} = 15.5 mN/m) to hexadecane (γ_{lv} = 27.5 mN/m), rapeseed oil (γ_{lv} = 35.5 mN/m), and diiodomethane (γ_{lv} = 50.8 mN/m) represent a set of nonpolar liquids; whereas dimethyl sulfoxide (γ_{lv} = 44 mN/m), ethylene glycol (γ_{lv} = 47.7 mN/m), and water (γ_{lv} = 72.1 mN/m) have polar natures. When compared with the extrapolated Zisman line (■, R^2 = 0.04), the Girifalco−Good curve (- - ■) is a much better fit (R^2 = 0.88) to the advancing contact-angle data

over the whole range of liquid-surface tensions, barring the two outliers, water (γ_{lv} = 72.1 mN/m) and ethylene glycol (γ_{lv} = 47.7 mN/m), which lie significantly below the curve. Statistical analysis based on the residuals between the best-fit predictions and measured values of cos θ_{adv} are summarized in the Supporting Information (Figures S1 and S2).

One of the main sources of uncertainty with Zisman analysis is the large extrapolation of the best-fit line to $\theta_{adv} \rightarrow 0$ that is typically required to estimate the value of γ_c. In the Girifalco–Good analysis, such an extrapolation is avoided. If a liquid (with surface tension γ^*_{lv}) is found such that it forms an equilibrium contact angle, $\theta_E \approx 90°$, then assuming that $\varphi_{sl} = 1$, the solid-surface energy can be found by solving eq 1, which yields $\gamma_{sv} = \gamma^*_{lv}/4$. Even if such a liquid cannot be found, γ_{sv} can be estimated by interpolation using two liquids (say 1 and 2) if $\theta_{E,1} > 90°$ and $\theta_{E,2} < 90°$. The location, shape, and curvature of the Girifalco–Good curve are an embodiment of the solid-surface energy (γ_{sv}), and in Zisman analysis, it is γ_c. The solid-surface energy (γ_{sv}) can also be represented as the intercept where the extrapolated Girifalco–Good curve intersects the cos $\theta_{adv} = 1$ line [γ_{sv} = 9.3 mN/m in this case].

Because the Girifalco–Good curve has positive curvature (i.e., it is concave "upward"), the Zisman critical surface tension always tends to underestimate the solid-surface energy ($\gamma_c < \gamma_{sv}$) determined from Girifalco–Good analysis. The Girifalco–Good relation (eq 1) can be rewritten in the form $\cos\theta_E = -1 + 2\phi_{sl}\sqrt{\gamma_{sv}/\gamma_{lv}}$, which can be further expressed as a Taylor series when $\gamma_{lv}/\gamma_{sv} \rightarrow 1^+$ in terms of $(\gamma_{lv}/\gamma_{sv} - 1)$, as shown in eq 2 (assuming $\varphi_{sl} = 1$, a good assumption for alkanes) (22).

$$\cos\theta_E = 1 - \left(\frac{\gamma_{lv}}{\gamma_{sv}} - 1\right) + \frac{3}{4}\left(\frac{\gamma_{lvv}}{\gamma_{sv}} - 1\right)^2 - \frac{5}{8}\left(\frac{\gamma_l}{\gamma_{sv}} - 1\right)^3 + \frac{35}{64}\left(\frac{\gamma_{lv}}{\gamma_{sv}} - 1\right)^4 - \ldots \quad (2)$$

This series converges only if $(\gamma_{lv}/\gamma_{sv} - 1) < 1$, i.e., $\gamma_{lv} < 2\gamma_{sv}$. The Taylor series can be truncated after the second term to get a linear relation between cos θ_E and γ_{lv} (eq 3), and the absolute value of the slope of this line is expected to be the inverse of the solid-surface energy (γ_{sv})

$$\cos\theta_E \approx 1 - \left(\frac{\gamma_{lv}}{\gamma_{sv}} - 1\right) \quad (3)$$

This linearization is valid only if the quadratic term is considerably smaller (ca. 10%) compared to the linear term. This condition restricts the range of liquid surface tensions $(\gamma_{lv}/\gamma_{sv}) < 1.13$ for which the linearization is valid, therefore in general, this linearization should be avoided. Johnson and Dettre have reported the value of the Zisman slope along with the intercept (γ_c) as a more complete indicator of the solid-surface energy (44). The absolute value of the Zisman slope equals the reciprocal of the Zisman critical surface tension (i.e., $\partial\cos\theta_E/\partial\gamma_{lv} = -1/\gamma_{sv}$). Slopes in the range of

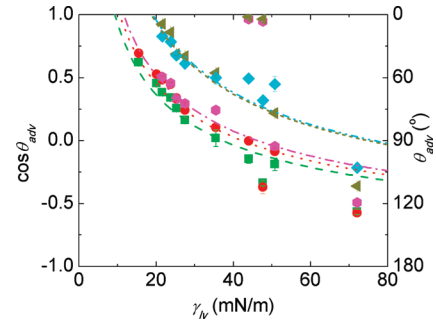

FIGURE 4. Variation in advancing contact angles (θ_{adv}) for T_8 cages surrounded by various fluorinated chains is summarized in this figure. Cosine of advancing contact angles (θ_{adv}) for droplets of water (γ_{lv} = 72.1 mN/m), diiodomethane (γ_{lv} = 50.8 mN/m), ethylene glycol (γ_{lv} = 47.7 mN/m), dimethyl sulfoxide (γ_{lv} = 44 mN/m), rapeseed oil (γ_{lv} = 35.5 mN/m), hexadecane (γ_{lv} = 27.5 mN/m), dodecane (γ_{lv} = 25.3 mN/m), decane (γ_{lv} = 23.8 mN/m), octane (γ_{lv} = 21.6 mN/m), heptane (γ_{lv} = 20.1 mN/m), and pentane (γ_{lv} = 15.5 mN/m) on a spin-coated film on a flat silicon wafer are plotted against the surface tension of contacting liquids (γ_{lv}). Solid-surface energy for fluorodecyl T_8 (γ_{sv} = 9.3 mN/m, ■), fluorooctyl T_8 (γ_{sv} = 10.6 mN/m, ●), fluorohexyl T_8 (γ_{sv} = 11.6 mN/m, ◆), fluoropropyl T_8 (γ_{sv} = 18.7 mN/m, ▲), and hexafluoroisbutyl T_8 (γ_{sv} = 19.1 mN/m, ♦) is estimated by the extrapolation of the best fit Girifalco–Good curve.

−0.035 to −0.050 $(mN/m)^{-1}$ were reported and the absolute value of the slope tends to increase with increasing γ_c (44). This trend is contradictory to the linear form of the truncated Taylor series expansion of the Giriflco–Good equation. Therefore, the slope of the Zisman line does not provide a complete description of the solid-surface energy (γ_{sv}).

The Girifalco–Good framework was also applied to smooth spin-coated surfaces prepared from the other T_8 molecules and the values of the solid-surface energy (γ_{sv}) were computed from the advancing contact-angle data (Figure 4). The calculated values of the solid-surface energy monotonically increase from γ_{sv} = 9.3 to 18.7 mN/m as the length of the fluorinated side chain decreases from fluorodecyl T_8 (■) to fluoropropyl T_8 (▲). These values follow a similar trend to that of the critical surface tension (γ_c), but as expected, there is a lack of quantitative agreement between the two.

A close-packed monolayer of $-CF_3$ moieties has the lowest known solid-surface energy ($\gamma_{sv} \approx 6.7$ mN/m) (19, 45). The side-chains of the fluoroalkylated molecules under consideration terminate with $-CF_3$ groups that are backed by $-CF_2-$ groups, with surface energies in the range of $\gamma_{sv} \approx 18–20$ mN/m (36). As the length of the perfluorinated chain increases, close packing of the chains becomes more favorable and consequently liquid-induced molecular reorganization at the surface becomes restricted. For fluorodecyl T_8 with the longest perfluorinated chain (seven $-CF_2-$ groups), predominantly $-CF_3$ groups are presented at the surface and the surface energy remains quite low (γ_{sv} = 9.3 mN/m). However, as the length of the fluorinated chain decreases, the tendency to chain alignment and crystallization reduces and the chains at the solid–liquid interface become more susceptible to liquid-induced reorganization. Consequently, the underlying higher surface energy moieties ($-CF_2-$ and $-CH_2-$ groups) are exposed to the contacting liquid, and γ_{sv} increases significantly from the value γ_{sv} = 9.3 mN/m, which is close to that of a $-CF_3$ monolayer.

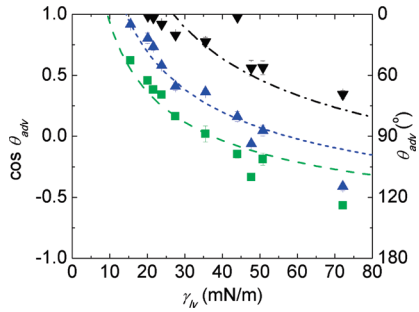

FIGURE 5. Variation in advancing contact angles (θ_{adv}) for various -Si/O- moieties surrounded by 1*H*,1*H*,2*H*,2*H*-heptadecafluorodecyl chains is summarized. Cosine of advancing contact angles (θ_{adv}) for droplets of water (γ_{lv} = 72.1 mN/m), diiodomethane (γ_{lv} = 50.8 mN/m), ethylene glycol (γ_{lv} = 47.7 mN/m), dimethyl sulfoxide (γ_{lv} = 44 mN/m), rapeseed oil (γ_{lv} = 35.5 mN/m), hexadecane (γ_{lv} = 27.5 mN/m), dodecane (γ_{lv} = 25.3 mN/m), decane (γ_{lv} = 23.8 mN/m), octane (γ_{lv} = 21.6 mN/m), heptane (γ_{lv} = 20.1 mN/m), and pentane (γ_{lv} = 15.5 mN/m) on a spin-coated film on a flat silicon wafer are plotted against the surface tension of contacting liquids (γ_{lv}). Solid-surface energy for fluorodecyl T_8 (γ_{sv} = 9.3 mN/m, ■), fluorodecyl Q_4 (γ_{sv} = 14.3 mN/m, ▲), and fluorodecyl M_2 (γ_{sv} = 26.8 mN/m, ▼) is estimated by the extrapolation of the best fit Girifalco−Good curve.

It was also noted that some high surface tension liquids like dimethyl sulfoxide (γ_{lv} = 44 mN/m) or ethylene glycol (γ_{lv} = 47.7 mN/m) fully wet ($\theta_E \rightarrow 0°$) the fluorohexyl and fluoropropyl T_8 surfaces, even though $\gamma_{lv} \gg \gamma_c$. This unexpected behavior is due to specific polar interactions across the solid−liquid interface and it can be understood by careful examination of the Girifalco−Good framework.

In one set of molecules, the T_8 cage structure was kept constant and the length of the perfluorinated side chain was changed (Figure 4). It was found that fluorodecyl T_8, with the longest perfluorinated side chain, had the lowest solid-surface energy (γ_{sv}) among the T_8 molecules. Therefore, in a second set of molecules, the fluorodecyl side chain was kept constant but the −Si/O− architecture was changed from the T_8 cage (■) to a Q_4 ring (▲) as well as a linear chain molecule (▼, M_2). The solid-surface energy (γ_{sv}) increased from 9.3 mN/m for the fluorodecyl T_8, to 14.3 mN/m for fluorodecyl Q_4, and finally to 26.8 mN/m for fluorodecyl M_2 (Figure 5). This trend is consistent with the variation in the corresponding critical surface tensions (γ_c) obtained from Zisman analysis. In this set of molecules, the perfluorinated side chain was held constant; therefore changes in the −Si/O− architecture are the only possible cause for the change in wettability. For the fluorodecyl M_2 molecules, the relative ease of access to the high-surface-energy −Si−O−Si− moiety is expected to be the reason for its high solid-surface energy. The reason for the difference in wettability of the fluorodecyl T_8 and Q_4 molecules is provisionally attributed to the presence of the −Si/O− cage.

According to the Girifalco−Good framework, the total surface energy can be divided into a dispersion (or nonpolar, γ^d) and a polar (γ^p) component. Subsequently, Girifalco, Good, and co-workers expressed the polar component of a solid (γ^p_{sv}) or a liquid (γ^p_{lv}) in terms of hydrogen-bond-donating (or acidic, γ^+) and hydrogen-bond-accepting (or basic, γ^-) components (as shown in eq 4)

$$\gamma_{lv} = \gamma^d_{lv} + \gamma^p_{lv} = \gamma^d_{lv} + 2\sqrt{\gamma^+_{lv}\gamma^-_{lv}}$$
$$\gamma_{sv} = \gamma^d_{sv} + \gamma^p_{sv} = \gamma^d_{sv} + 2\sqrt{\gamma^+_{sv}\gamma^-_{sv}} \quad (4)$$

Liquids such as acetone (γ_{lv} = 25.2 mN/m) or dimethyl sulfoxide (γ_{lv} = 44 mN/m) have an oxygen atom attached to an electropositive atom; therefore, the oxygen can donate its lone pair of electrons or accept hydrogen bonds. These liquids do not have any acidic protons, and therefore have negligibly small values of hydrogen-bond-donating components of surface energy (γ^+_{lv}). Such liquids with one predominant polar component are said to be monopolar liquids. Liquids like ethylene glycol (γ_{lv} = 47.7 mN/m) and glycerol (γ_{lv} = 66 mN/m) have both (a) an electronegative atom like oxygen that can accept hydrogen bonds, and (b) a hydrogen atom bonded to electronegative oxygen atom, which can be easily donated. Therefore, such liquids have appreciable values of both the polar components (γ^+_{lv},γ^-_{lv}), and they are commonly termed bipolar liquids. Values of the surface-energy components are known (tabulated in the Supporting Information) based on water as a standard state with $\gamma^+_{lv} = \gamma^-_{lv}$ = 25.5 mN/m. Some researchers have recently argued that for water $\gamma^+_{lv}/\gamma^-_{lv}$ = 6.5, based on the shifts in the absorption wavelengths of solvatochromic dyesv (46), but we have used the former standard state because of the availability of surface energy component data in this reference frame. Finally, it is important to note that the magnitude of acidic (γ^+_{sv}) and basic components (γ^-_{sv}) of the solid-surface energy depends on the choice of the standard state, whereas the magnitude of the total polar ($\gamma^p_{sv} = 2\sqrt{\gamma^+_{sv}\gamma^-_{sv}}$)and dispersion component (γ^d_{sv})is independent of the standard state.

Two molecules of a bipolar liquid can have dispersion (nonpolar) as well as polar cohesive interactions with each other; and due to the presence of these additional polar interactions, the surface tension (γ_{lv}) and work of cohesion ($W^c_{ll} = 2\gamma_{lv}$) for bipolar liquids tends to be higher than for nonpolar or monopolar liquids (Figure 6). A droplet of a bipolar liquid can interact with a nonpolar solid only through dispersion adhesive interactions, and consequently the work of adhesion (W^a_{sl}) tends to be lower for a bipolar liquid on a nonpolar solid. Therefore, for a droplet of bipolar liquid (like water and ethylene glycol) on a nonpolar solid, the parameter $\varphi_{sl} = W^a_{sl}/\sqrt{W^c_{ss}W^c_{ll}} < 1$ (47). In Figure 3−5, we fitted eq 1 to the advancing contact-angle data, assuming $\varphi_{sl} = 1$, but we now recognize that $\varphi_{sl} < 1$ for water and ethylene glycol on nonpolar surfaces. Therefore, these points corresponding to bipolar liquids are not expected to lie on the best-fit curve (eq 1). The statistical Dixon Q-test was used to decide whether to use the water and/or ethylene glycol data for fitting eq 1. On the basis of the magnitude of the residuals and the Q-test tables, both water and ethylene glycol data were rejected for fitting eq 1 with a 95% confidence for the fluorodecyl T_8 surface. A similar statistical exercise was carried out for all the solid surfaces and the "best-fit" plots in Figure 4 and 5 are based on the liquids that satisfy the Dixon Q-test with 95% confidence (data shown in the

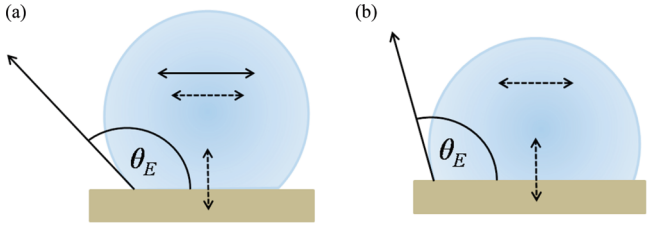

FIGURE 6. Schematic of (a) a bipolar and (b) a monopolar or a nonpolar liquid droplet on a nonpolar solid surface is shown. The dotted arrows indicate a nonpolar (dispersion) interaction and the filled arrows (↔) indicate a polar interaction. A bipolar liquid has both polar and nonpolar cohesive interactions, whereas a monopolar or a nonpolar liquid has only nonpolar cohesive interactions. Consequently, for the same values of liquid surface tension (γ_{lv}) and solid-surface energy (γ_{sv}), a droplet of a bipolar liquid forms higher equilibrium contact angle (θ_E) compared to a droplet of either a monopolar or a nonpolar liquid. (This figure is adapted from the book by Van Oss (47).)

Supporting Information). Moreover, from the value of the best-fit predicted and experimentally measured contact angles, the parameter φ_{sl} can be computed to be 0.60 for water and 0.75 for ethylene glycol on the fluorodecyl T_8 surface. For monopolar or nonpolar liquids on nonpolar solids, both the cohesive and adhesive interactions are dispersive; therefore, the parameter φ_{sl} is expected to be close to unity and it is found to be $0.95 \leq \varphi_{sl} \leq 1.05$ for such liquids on nonpolar solids.

The advancing contact angles for dimethyl sulfoxide and ethylene glycol droplets were found to have surprisingly low contact angles ($\theta_{adv} < 15°$) on fluorohexyl T_8, fluoropropyl T_8, and fluorodecyl M_2 surfaces (Figures 4 and 5). These low contact angles are believed to occur due to a strong specific polar interaction ($\varphi_{sl} \gg 1$) across the solid−liquid interface. These anomalously low contact angles were excluded from the fitting to obtain the solid-surface energies. If a solid is soluble in a probing liquid, the contact angles of such a solid−liquid combination cannot be used for the estimation of solid-surface energy (γ_{sv}). Solid−liquid pairs for which solubility is questionable are marked in red in Tables S4 and S5 in the Supporting Information. However, we feel that probing a solid surface using a set of polar and nonpolar liquids is a good approach to estimate solid-surface energy (γ_{sv}).

The solid−liquid work of adhesion (W^a_{sl}) can be written in terms of the individual components of the surface energy of the solid and contacting liquid (39, 42, 43)

$$W^a_{sl} = \gamma_{lv}(1 + \cos\theta_E) = 2[\sqrt{\gamma^d_{sv}\gamma^d_{lv}} + \sqrt{\gamma^+_{sv}\gamma^-_{lv}} + \sqrt{\gamma^-_{sv}\gamma^+_{lv}}] \quad (5)$$

Note that the first term on the right-hand side of eq 5 ($\sqrt{\gamma^d_{sv}\gamma^d_{lv}}$) has the same form as eq 1, but the other two terms appear in the form of a cross product. The hydrogen-bond-donating component of the solid (γ^+_{sv}) interacts with the hydrogen-bond -accepting component of the liquid (γ^-_{lv}) and vice versa. If either the solid or the liquid is purely nonpolar, then these polar interactions vanish and eq 5 simplifies to eq 1. The individual contributions to the liquid surface tension ($\gamma^d_{lv}, \gamma^+_{lv}, \gamma^-_{lv}$) are known for a few standard liquids (see the Supporting Information). Therefore by measuring the equilibrium contact angles of (at least) three contacting liquid droplets, the three unknowns in eq 5 ($\gamma^d_{sv}, \gamma^+_{sv}, \gamma^-_{sv}$) can be obtained by solving a linear system of three equations [A][x] = [b], given by eq 6.

$$2\begin{bmatrix} \sqrt{\gamma^d_{lv,1}} + \sqrt{\gamma^-_{lv,1}} + \sqrt{\gamma^+_{lv,1}} \\ \sqrt{\gamma^d_{lv,2}} + \sqrt{\gamma^-_{lv,2}} + \sqrt{\gamma^+_{lv,2}} \\ \sqrt{\gamma^d_{lv,3}} + \sqrt{\gamma^-_{lv,3}} + \sqrt{\gamma^+_{lv,3}} \end{bmatrix}\begin{bmatrix} \gamma^d_{sv} \\ \gamma^+_{sv} \\ \gamma^-_{sv} \end{bmatrix} = \begin{bmatrix} \gamma_{lv,1}(1 + \cos\theta_{E,1}) \\ \gamma_{lv,2}(1 + \cos\theta_{E,2}) \\ \gamma_{lv,3}(1 + \cos\theta_{E,3}) \end{bmatrix} \quad (6)$$

The relative error in the contact angle measurements (the right-hand side of eq 6) is amplified by the condition number of matrix [A], and therefore the contacting liquids are chosen such that the matrix [A] is not ill-conditioned or it has as low a condition number as possible (46, 48). Dodecane (γ_{lv} = 25.3 mN/m), chloroform (γ_{lv} = 27.5 mN/m), and acetone (γ_{lv} = 25.2 mN/m) were chosen as a set of contacting liquids. All the three liquids have similar values of surface tensions but different polarities. Acetone has a strongly monopolar hydrogen-bond-accepting component ($\gamma^+_{lv} = 0, \gamma^-_{lv} = 24$ mN/m), and chloroform has a weekly monopolar hydrogen-bond-donating component (γ^+_{lv} = 3.8, γ^-_{lv} = 0 mN/m), whereas dodecane is completely nonpolar ($\gamma^+_{lv} = \gamma^-_{lv} = 0$). Even though both acetone and chloroform are polar, due to their monopolar nature, the polar component of surface energy is zero ($\gamma^p_{lv} = 2\sqrt{\gamma^+_{lv}\gamma^-_{lv}} = 0$). The condition number of the prefactor matrix [A] is reasonably small (7.2), and therefore this set of liquids can be used successfully to evaluate the individual components of the solid-surface energy. All three liquids are expected to have similar contact angles on nonpolar solids (i.e., solids with $\gamma^+_{sv} = \gamma^-_{sv} = 0$), as the last two terms of eq 5 vanish and the interactions across solid−liquid are purely dispersive. Indeed, dodecane (θ_{adv} = 75 ± 2°, θ_{rec} = 60 ± 4°, ◨), acetone (θ_{adv} = 71 ± 2°, θ_{rec} = 59 ± 4°, ⬒), and chloroform droplets (θ_{adv} = 73 ± 2°, θ_{rec} = 54 ± 4°, ⬓) all form similar contact angles on fluorodecyl T_8, which is a completely nonpolar molecule (Figure 7a). As the polarity of the surfaces increases from fluorodecyl T_8 to fluorooctyl T_8, and finally fluorodecyl Q_4, the acetone and chloroform droplets form much lower contact angles in comparison with dodecane droplets. For example, on the fluorodecyl Q_4 surface (Figure 7c), the dodecane contact angles (θ_{adv} = 62 ± 2°, θ_{rec} = 17 ± 2°, ◭) are much larger than those measured for acetone (θ_{adv} = 30 ± 1°, $\theta_{rec} \approx 0°$, top-shaded triangle) or chloroform (θ_{adv} = 29 ± 4°, θ_{rec} = 15 ± 3°, bottom-shaded triangle). Therefore, it is vital to know about the polarity of the contacting liquids and solids when evaluating the equilibrium contact angles and solid-surface energies (γ_{sv}).

Highly fluorinated species possess surfaces with relatively low polarity and low solid-surface energy. The reason for this can be understood by looking at the unusual characteristics of fluorine. Fluorine is the most electronegative element of the periodic Table (3.98 on the Pauling scale). Carbon (2.55)

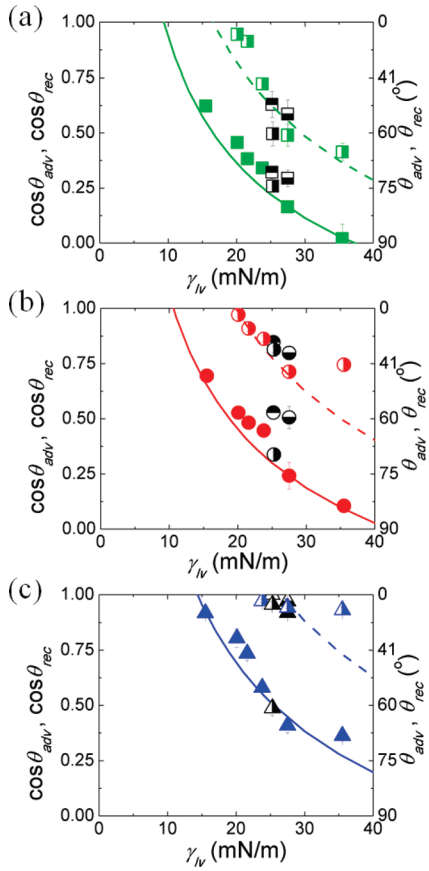

FIGURE 7. Variation in advancing and receding contact angles (θ_{adv}, θ_{rec}) is summarized for (a) fluorodecyl T_8 (green ■, ◨), (b) fluorooctyl T_8 (red ●, ◑), and (c) fluorodecyl Q_4 (blue ▲, ◭). Cosine of advancing and receding contact angles (θ_{adv}, θ_{rec}) for droplets of hexadecane (γ_{lv} = 27.5 mN/m), dodecane (γ_{lv} = 25.3 mN/m), decane (γ_{lv} = 23.8 mN/m), octane (γ_{lv} = 21.6 mN/m), heptane (γ_{lv} = 20.1 mN/m), pentane (γ_{lv} = 15.5 mN/m), chloroform (γ_{lv} = 27.5 mN/m), and acetone (γ_{lv} = 25.2 mN/m) on a spin-coated film on a flat silicon wafer are plotted against the surface tension of contacting liquids (γ_{lv}). Solid-surface energy is estimated by substituting the values of the contact angles with dodecane (black ◨, ◑, ◭), chloroform (black ⬓) and acetone droplets (black ⬒) in the Girifalco−Good equation and summarized in Table 1.

is significantly less electronegative. Consequently, a C−F bond is polar ($C^{\delta+}-F^{\delta-}$) and acquires partial ionic character. A carbon atom bonded to three fluorine atoms ($-CF_3$) is significantly electron deficient. The only way to reduce the dipole moment between this α carbon ($-CF_3$) and the adjacent β carbon is by placing electronegative atoms on the β carbon as well. By perfluorinating a large number of successive carbon atoms, the $-CF_2-CH_2-$ dipole is buried deep within the molecule. Therefore, fluorodecyl T_8 and other molecules with long fluorinated side chains exhibit an almost negligible polar component of solid-surface energy ($\gamma_{sv}^p \approx 0$). Furthermore, because of the small size (van der Waals radius, r = 1.47 Å), the polarizability of a fluorine atom is small, and it is difficult to create fluctuating dipoles involving fluorine atoms. The interaction energy arising from London forces varies as the square of the polarizability. Therefore, the dispersion component of the solid-surface energy (γ_{sv}^d) is also small for fluorinated species (49). Intuitively, the high electronegativity of fluorine makes it an ideal candidate for accepting hydrogen bonds,and fluorinated species might be expected to have a high value of γ_{sv}^-. However, in practice, because of the small size and small polarizability, a fluorine atom holds the three lone pairs of electrons extremely tightly and is a poor hydrogen bond acceptor. The hydrogen bonds formed by fluorinated species are weaker in strength (typically 1/4th of the bond energy of a −C═O · · · H−OR bond) (50). On the contrary, hydrogen (2.20) and carbon (2.55) have similar electronegativities and form nonpolar bonds. Because of the relatively higher polarizability of hydrogen, the dispersion component of the solid-surface energy for hydrocarbons tends to be higher than corresponding fluorocarbons.

Using eq 5 and the set of three liquids mentioned above (acetone, chloroform, and dodecane), we estimated the solid-surface energy for various fluoroalkylated silicon-containing molecules (summarized in Table 2). For the fluorodecyl T_8 POSS cages, this value of surface energy agreed (within experimental error) with the value estimated using eq 1. However, the three probing liquids possess low surface tension values ($\gamma_{lv} \approx$ 25 to 27 mN/m) and wet most nonfluorinated surfaces with values of γ_{sv} > 25 mN/m. Moreover, the relative error in the measurement of small contact angles is always large. Therefore, a set of probing liquids with higher surface tension values is needed to accurately probe higher energy surfaces. Water (γ_{lv} = 72.1 mN/m), diiodomethane (γ_{lv} = 50.8 mN/m), and dimethyl sulfoxide (γ_{lv} = 44 mN/m) constitute such a set with high values of liquid surface tension (and give rise to a small condition number for the matrix [A], cond(A) = 4.58). Using this set of liquids, a broader range of surfaces (γ_{sv} < 40 mN/m) can be analyzed using the Girifalco−Good method (see Tables 2 and 3). For fluorohexyl, fluoropropyl, and hexafluoro-i-butyl T_8 surfaces, solid-surface energy values obtained using these three high-surface-tension liquids (column 4 of Table 2) did not match the previously obtained values (columns 2 and 3). To diagnose the reason for this mismatch, the magnitudes of the individual components of the solid-surface energy must be considered (as summarized in Table 3). The values of the dispersion component of the solid-surface energy (γ_{sv}^d, given in column 5 of Table 3) match well with the solid-surface energy (γ_{sv}, column 3 of Table 3) calculated using eq 1.

The dispersion component of the solid-surface energy (calculated in Table 3) increased monotonically from fluorodecyl T_8 (γ_{sv}^d = 8.7 mN/m) to hexafluoro-i-butyl T_8 (γ_{sv}^d = 26.8 mN/m), whereas the polar component (γ_{sv}^p) does not follow any clear trend. The fluoroalkylated T_8 molecules have two methylene groups [one methylene and one methyne group in case of haxafluoro-i-butyl T_8] connecting the −Si−O− cage with the fluoroalkyl chain (see structure in Table 1). Methylene groups are nonpolar, but due to the higher polarizability of a $-CH_2-$ moiety (as compared with a $-CF_2-$ moiety), the dispersion component of the solid-surface energy tends to be higher (γ_{sv}^d for polyethylene ≈ 30−32 mN/m, versus γ_{sv}^d = 18−20 mN/m for PTFE and 6.7 mN/m for a monolayer of $-CF_3$ groups). Therefore, this increase in γ_{sv}^d of the T_8 molecules is attributed to higher

Table 2. Computed Values of Solid-Surface Energy (γ_{sv} mN/m) for Various Fluoroalkylated Silicon-Containing Moieties[a]

γ_{sv} (mN/m) based on contact angles (deg) of the probing liquids	all liquids[b] (eq *1* with $\varphi_{sl} = 1$)	dodecane, acetone, and chloroform (eq *5*)	diiodomethane, dimethyl sulfoxide, and water (eq *5*)
fluorodecyl T_8	9.3	10.2	8.8
fluorooctyl T_8	10.6	13.6	10.9
fluorohexyl T_8	11.6	26.8	47.4
fluoropropyl T_8	18.7	21.4	38.4
hexafluoro-i-butyl T_8	19.1	19.8	26.9
fluorodecyl T_8	9.3	10.2	8.8
fluorodecyl Q_4	14.3	20.1	14.9
fluorodecyl M_2	26.8		39.7

[a] Assuming a typical error in contact angle measurement ($\Delta\theta \approx 2°$), and from the condition number of the transformation matrix in the system of linear equations, a 15% relative error ($\delta\gamma_{sv}/\gamma_{sv}$) is expected in the computed values of the surface energies. [b] All liquids include a set of n-alkanes from pentane to hexadecane, rapeseed oil, dimethyl sulfoxide, ethylene glycol, diiodomethane, and water.

Table 3. Computed Values of the Dispersion (γ_{sv}^{d}), Acidic (γ_{sv}^{+}), and Basic (γ_{sv}^{-}) Components of Solid-Surface Energy (mN/m) for Various Fluoroalkylated Silicon-Containing Moieties

	alkanes (Zisman analysis)	all liquids[b] (eq 1 with $\varphi_{sl} = 1$)	diiodomethane, dimethyl sulfoxide and water (eq *5*)				
	γ_c	γ_{sv}	γ_{sv}	dispersion (γ_{sv}^{d})	polar (γ_{sv}^{p})	acidic (γ_{sv}^{+})	basic (γ_{sv}^{-})
fluorodecyl T_8	5.5	9.3	8.8	8.7	0.1	0.04	0.1
fluorooctyl T_8	7.4	10.6	10.9	10.6	0.3	0.2	0.1
fluorohexyl T_8	8.5	11.6	47.4	11.4	36.0	20.8	15.6
fluoropropyl T_8	19.7	18.7	38.4	19.1	19.3	11.8	7.9
hexafluoro-i-butyl T_8	17.7	19.1	26.9	26.8	0.1	0.002	0.8
fluorodecyl T_8	5.5	9.3	8.8	8.7	0.1	0.04	0.1
fluorodecyl Q_4	14.5	14.3	14.9	14.5	0.8	0.0	0.2
fluorodecyl M_2	19.6	26.8	39.7	30.9	8.8	2.0	9.7

interaction of the contacting liquids with the underlying $-CH_2-CH_2-$ and $(-CF_2-)_n$ groups. As the length of the perfluorinated chain decreases, the crystalline-like packing of the side chains becomes unfavorable and the underlying $-CF_2-$ and $-CH_2-$ groups start contributing to the total solid-surface energy.

Similarly, when we compare the fluorodecyl T_8, Q_4, and M_2 molecules, we find that γ_{sv}^{d} increases monotonically from a T_8 cage (8.7 mN/m) to a Q_4 ring (14.5 mN/m) and finally to a M_2 straight chain (30.9 mN/m) and this increase in the dispersion component of the solid-surface energy accounts for most of the increase in the total surface energy (γ_{sv}). The T_8 cage structure seems to achieve an optimal packing of the eight fluorodecyl chains, which results in very restricted ability to rearrange these chains when in contact with probing liquids. As a consequence, the fluorodecyl T_8 cage has the lowest solid-surface energy among all the molecules tested. The behavior of T_8 surfaces with fluorinated chains longer than the fluorodecyl group (i.e., greater in length than $-(CF_2)_7CF_3$) is still an open question. Currently, fluorododecyl and fluorotetradecyl T_8 synthesis is underway and the systematic analysis of their wettability will be the scope of a future investigation.

The main objective of this paper was to estimate the solid-surface energy of the native solid surface. The discussion above is based on calculations of the solid-surface energy obtained by substituting the advancing contact angle (θ_{adv}) in place of the equilibrium contact angle (θ_E) in the governing equations. The advancing contact angle (θ_{adv}) is the local value of the contact angle formed by a liquid droplet when it touches the solid surface for the first time, so the advancing contact angle (θ_{adv}) is the physically more relevant measurement to use rather than the receding contact angle (θ_{rec}) in the context of determining solid-surface energies. Although uncontrolled local chemical inhomogeneities and dust contamination can contribute to contact angle hysteresis, we believe that the most important factor in the carefully controlled spin-coated flat surfaces studied in the present work is reorganization or reconstruction of the solid surface as a result of contact with the probing liquid. As a result, a finite contact angle hysteresis ($\Delta\theta = \theta_{adv} - \theta_{rec}$) was observed for all the molecules studied here. Substituting the advancing contact angles (θ_{adv}) on a flat surface in place of the equilibrium contact angle (θ_E), into the Girifalco–Good equation leads to a value of solid-surface energy (say $\gamma_{sv,a}$), whereas substituting receding contact angles (θ_{rec}) yields a higher value of solid-surface energy (say $\gamma_{sv,r} > \gamma_{sv,a}$), i.e., $\cos\theta_{adv} = -1 + 2\phi_{sl}\sqrt{(\gamma_{sv,a})/(\gamma_{lv})}$ and $\cos\theta_{rec} = -1 + 2\phi_{sl}\sqrt{(\gamma_{sv,r})/(\gamma_{lv})}$. If the difference between $\gamma_{sv,r}$ and $\gamma_{sv,a}$ is small, a low-energy solid surface has the desirable attribute of being able to resist reorganization in the presence of the contacting liquid. As shown in Table S6 of the Supporting Information, fluorodecyl T_8 exhibits the lowest value of $\gamma_{sv,r} - \gamma_{sv,a}$ (≈7 mN/m). Fluorodecyl Q_4 and fluorodecyl M_2 molecules are more susceptible to rearrangements in contact with probing liquids, as indicated by comparatively higher values of $\gamma_{sv,r} - \gamma_{sv,a}$, 12.2 and 9.0 mN/m, respectively. In the case of molecules with a T_8 cage, the fluoropropyl molecule has

equally low value of $\gamma_{sv,r} - \gamma_{sv,a}$ as that measured for fluorodecyl T_8, though the inherent solid-surface energy is much higher for the fluoropropyl T_8 molecule ($\gamma_{sv} = 18.7$ vs 9.3 mN/m for fluorodecyl T_8). (See the Supporting Information, Table S6, for more details on the analysis of contact angle hysteresis ($\gamma_{sv,r} - \gamma_{sv,a}$) on various solid surfaces.)

Thus, we note that the special character of fluorodecyl POSS (lowest solid-surface energy $\gamma_{sv} = 9.3$ mN/m along with maximum resistance to solid-surface reconstruction and thus low contact angle hysteresis) apparently arises from the favorable combination of the cage structure and the fluorodecyl side chains. The latter contribute to an unusually low value of dispersive contribution to the solid-surface energy while simultaneously reducing polar contributions to nearly zero. The cage structure is relatively inflexible toward molecular reorganization compared to the ring or linear analogs. Whether or not fluorodecyl side chain represents the optimal substituent remains an open question. A plot of solid-surface energy (γ_{sv}) versus cage substituent chain length (see Figure S4 in the Supporting Information) suggests that a minimum may not yet have been achieved with the fluorodecyl substituent. Synthesis of the dodecyl and tetradecyl analogs is now underway to explore this unanswered question. We note, however, that very long fluoroalkyl chains on the POSS cage should eventually produce PTFE-like surface energies in the range of $\gamma_{sv} = 18-20$ mN/m, well above the value of $\gamma_{sv} = 9.3$ mN/m found here for the fluorodecyl cage molecule.

CONCLUSIONS

The solid-surface energy (γ_{sv}) plays a key role in controlling the equilibrium contact angle (θ_E) and subsequently the robustness (P_b) of a liquid droplet and apparent contact angle (θ^*) on a textured surface that enables a solid−liquid−air composite interface to be established. Smooth fluorodecyl POSS surfaces lead to one of the highest known equilibrium contact angles (θ_E) at the 3-phase contact line. To investigate why fluorodecyl POSS performs so well as a nonwetting coating, we synthesized a series of fluoroalylated silicon-containing molecules resembling fluorodecyl POSS. Their wettability characteristics were assessed using (1) Zisman analysis with a set of n-alkanes and (2) Girifalco−Good analysis using a broad range of polar and nonpolar liquids. Both the critical surface tension (γ_c) and the calculated value of solid-surface energy (γ_{sv}) follow the same trend: The solid-surface energy increased monotonically from $\gamma_{sv} = 9.3$ to $\gamma_{sv} = 18.7$ mN/m as the length of the perfluorinated chain was reduced from fluorodecyl to fluoropropyl T_8 POSS and as the dimensionality of the cage was reduced from 9.3 mN/m for fluorodecyl T_8 3D cage to 14.3 mN/m for fluorodecyl Q_4 ring and 26.8 mN/m for a fluorodecyl M_2 linear chain molecule. Hydrogen bond donating (γ^+), hydrogen bond accepting (γ^-), polar (γ^p) and dispersion components (γ^d) of the total solid-surface energy were also individually computed using two sets of probing liquids (dodecane, acetone, chloroform and water, diiodomethane, dimethyl sulfoxide, respectively). Of the fluorinated molecules tested so far, fluorodecyl T_8 has the lowest solid-surface energy ($\gamma_{sv} = 9.3$ mN/m) along with the lowest degree of surface reorganization, manifested through a lowest increment in the solid-surface energy ($\Delta\gamma_{sv} = 7.0$ mN/m) in contact with probing liquids. This desirable property probably arises because of the synergy between a rigid T_8 cage surrounded by long fluorodecyl side chains.

Acknowledgment. This research was supported by the Army Research Office (ARO) through Contract W911NF-07-D-0004. Financial support was also provided by the Air Force Office of Scientific Research and the Air Force Research laboratory, Propulsion Directorate. We thank Prof. Michael Rubner and the Institute of Soldier Nanotechnologies (ISN) at MIT for the use of various experimental facilities, Ms. Wui Siew Tan and Mr. Siddharth Srinivasan for help with the AFM characterization, and Dr. Adam J. Meuler for helpful discussion during the preparation of this manuscript.

Supporting Information Available: Raw contact angle data, quantification about the deviation of the contact angle data from the Zisman line and the Girifalco−Good curve, liquid surface-tension values used for solid-surface energy calculations, and computed values of the solid-surface energy (PDF). This material is available free of charge via the Internet at http://pubs.acs.org.

REFERENCES AND NOTES

(1) Lafuma, A.; Quéré, D. *Nat. Mater.* **2003**, *2*, 457–460.
(2) Ma, M.; Hill, R. M.; Rutledge, G. C. *J. Adhes. Sci. Technol.* **2008**, *22*, 1799–1817.
(3) Ma, M.; Mao, Y.; Gupta, M.; Gleason, K. K.; Rutledge, G. C. *Macromolecules* **2005**, *38*, 9742–9748.
(4) Michielsen, S.; Lee, H. J. *Langmuir* **2007**, *23*, 6004–6010.
(5) Ahuja, A.; Taylor, J. A.; Lifton, V.; Sidorenko, A. A.; Salamon, T. R.; Lobaton, E. J.; Kolodner, P.; Krupenkin, T. N. *Langmuir* **2008**, *24*, 9–14.
(6) Brewer, S. A.; Willis, C. R. *Appl. Surf. Sci.* **2008**, *254*, 6450–6454.
(7) Chhatre, S. S.; Choi, W.; Tuteja, A.; Park, K.-C.; Mabry, J. M.; McKinley, G. H.; Cohen, R. E. *Langmuir* **2010**, *26*, 4027–4035.
(8) Chhatre, S. S.; Tuteja, A.; Choi, W.; Revaux, A. l.; Smith, D.; Mabry, J. M.; McKinley, G. H.; Cohen, R. E. *Langmuir* **2009**, *25*, 13625–13632.
(9) Choi, W.; Tuteja, A.; Chhatre, S.; Mabry, J. M.; Cohen, R. E.; McKinley, G. H. *Adv. Mater.* **2009**, *21*, 2190–2195.
(10) Choi, W.; Tuteja, A.; Mabry, J. M.; Cohen, R. E.; McKinley, G. H. *J. Colloid Interface Sci.* **2009**, *339*, 208–216.
(11) Tuteja, A.; Choi, W.; Ma, M.; Mabry, J. M.; Mazzella, S. A.; Rutledge, G. C.; McKinley, G. H.; Cohen, R. E. *Science* **2007**, *318*, 1618–1622.
(12) Tuteja, A.; Choi, W.; Mabry, J. M.; McKinley, G. H.; Cohen, R. E. *Proc. Natl. Acad. Sci. U.S.A.* **2008**, 18200–18205.
(13) Tuteja, A.; Choi, W.; McKinley, G. H.; Cohen, R. E.; Rubner, M. F. *MRS Bull.* **2008**, *33*, 752–758.
(14) Hoefnagels, H. F.; Wu, D.; deWith, G.; Ming, W. *Langmuir* **2007**, *23*, 13158–13163.
(15) Leng, B.; Shao, Z.; de With, G.; Ming, W. *Langmuir* **2009**, *25*, 2456–2460.
(16) Marmur, A. *Langmuir* **2008**, *24*, 7573–7579.
(17) Cassie, A.; Baxter, S. *Trans. Faraday Soc.* **1944**, *40*, 546–551.
(18) Mabry, J.; Vij, A.; Iacono, S.; Viers, B. *Angew. Chem., Int. Ed.* **2008**, *47*, 4137–4140.
(19) Zisman, W. A. Relation of the Equilibrium Contact Angle to Liquid and Solid Construction. In *Contact Angle, Wettability, and Adhesion*; Fowkes, F. M., Ed.; Advances in Chemistry Series; American Chemical Society: Washington, D.C., 1964; Vol. 43.
(20) Owens, D. K.; Wendt, R. C. *J. Appl. Polym. Sci.* **1969**, *13*, 1741–1747.
(21) Good, R. J. *J. Colloid Interface Sci.* **1977**, *59*, 398–419.
(22) Good, R. J. *J. Adhes. Sci. Technol.* **1992**, *6*, 1269–1302.
(23) Iacono, S. T.; Vij, A.; Grabow, W.; Smith, D. W., Jr.; Mabry, J. M. *Chem. Commun.* **2007**, *499*, 2–4994.

(24) Goodwin, G. B.; Kenney, M. E. U.S. Patent 4824985, 1989.
(25) Teng, C. J.; Cai, G.; Weber, W. P. *J. Fluorine Chem.* **2004**, *125*, 1451–1455.
(26) Lentz, C. W. *Inorg. Chem.* **1964**, *3*, 574–579.
(27) Bernett, M. K.; Zisman, W. A. *J. Phys. Chem.* **1960**, *64*, 1292–1294.
(28) Bernett, M. K.; Zisman, W. A. *J. Phys. Chem.* **1973**, *77*, 2324–2328.
(29) Ellison, A. H.; Fox, H. W.; Zisman, W. A. *J. Phys. Chem.* **1953**, *57*, 622–627.
(30) Ellison, A. H.; Zisman, W. A. *J. Phys. Chem.* **1954**, *58*, 503–506.
(31) Ellison, A. H.; Zisman, W. A. *J. Phys. Chem.* **1954**, *58*, 260–265.
(32) Fox, H. W.; Hare, E. F.; Zisman, W. A. *J. Colloid Sci.* **1953**, *8*, 194–203.
(33) Schulman, F.; Zisman, W. A. *J. Colloid Sci.* **1952**, *7*, 465–481.
(34) Shafrin, E. G.; Zisman, W. A. *J. Phys. Chem.* **1962**, *66*, 740–748.
(35) Bernett, M. K.; Zisman, W. A. *J. Phys. Chem.* **1962**, *66*, 1207–1208.
(36) Fox, H. W.; Zisman, W. A. *J. Colloid Sci.* **1950**, *5*, 514–531.
(37) Fox, H. W.; Zisman, W. A. *J. Colloid Sci.* **1952**, *7*, 109–121.
(38) Fox, H. W.; Zisman, W. A. *J. Coll. Sci.* **1952**, *7*, 428–442.
(39) Chaudhury, M. K. *Mater. Sci. Eng., R* **1996**, *16*, 97–159.
(40) Girifalco, L. A.; Good, R. J. *J. Phys. Chem.* **1957**, *61*, 904–909.
(41) Good, R. J.; Girifalco, L. A. *J. Phys. Chem.* **1960**, *64*, 561–565.
(42) Van Oss, C. J.; Chaudhury, M. K.; Good, R. J. *Chem. Rev.* **1988**, *88*, 927–941.
(43) Van Oss, C. J.; Good, R. J.; Chaudhury, M. K. *Langmuir* **1988**, *4*, 884–891.
(44) Johnson, R. E.; Dettre, R. H. *Wetting of Low-Energy Surfaces*; Marcel Dekker: New York, 1993; p 1—74.
(45) Nishino, T.; Meguro, M.; Nakamae, K.; Matsushita, M.; Ueda, Y. *Langmuir* **1999**, *15*, 4321–4323.
(46) Volpe, C. D.; Siboni, S. *J. Colloid Interface Sci.* **1997**, *195*, 121–136.
(47) Van Oss, C. J. *Interfacial Forces in Aqueous Media*; Marcel Dekker: New York, 1994; pp 18—45.
(48) Shalel-Levanon, S.; Marmur, A. *J. Colloid Interface Sci.* **2003**, *262*, 489–499.
(49) Lemal, D. M. *J. Org. Chem.* **2004**, *69*, 1–11.
(50) O'Hagan, D. *Chem. Soc. Rev.* **2008**, *37*, 308–319.

AM100729J